Aviation Electronics, Information Technology, Telecommunications, Electricals, and Controls (AVITEC)
Vol. 8, No. 1, February 2026, pp. 1-9, p-ISSN 2685-2381, e-ISSN 2715-2626
http://dx.doi.org/10.28989/avitec.v8i1.3295

Research Article

Smart Airport Radar: Multimodal AI Classification of Aerial Threats with Communication Link Performance Evaluation

Nadhir Ibrahim Abdulkhaleq[1]* and Ahmed Saad Hussein[2]
[1]Department of Mobile Communication and Computing Engineering, College of Engineering, University of Information Technology and Communications, Iraq
[2]Computer Engineering Department, Al-Farabi University College, Iraq

Article Info

Article history:
Submitted August 17, 2025
Accepted November 7, 2025
Published November 21, 2025

Keywords:
UAV classification;
airport security;
multimodal features;
Support Vector Machine (SVM);
radar cross-section (RCS);
Signal-to-Noise Ratio (SNR).

ABSTRACT

The proliferation of small unmanned aerial vehicles (UAVs) near airports poses increasing risks to airspace safety and infrastructure security. This paper presents Smart Airport Radar, a simulation-based framework for classifying aerial threats — including drones, decoys, and birds — using multimodal AI features. The system emulates dynamic swarming behaviors and extracts five key descriptors — mean speed, heading variability, jerk, thermal signature, and radar cross-section (RCS) — to train a multiclass Support Vector Machine (SVM) classifier. Comparative analysis with a traditional RCS-based rule method shows the SVM achieving a classification accuracy of 93.33%, far outperforming the baseline at 20.00%. Radar-style trajectory visualizations and class-specific precision, recall, and F1-scores confirm the model's robustness and interpretability. Beyond sensing and classification, the framework incorporates a communication link performance evaluation, analyzing classification accuracy under varying Signal-to-Noise Ratio (SNR) levels. Results reveal that maintaining link quality above 15 dB SNR preserves near-optimal detection performance, bridging radar sensing with wireless communication reliability. With minimal computational overhead, high adaptability, and strong cross-domain relevance, the proposed system offers a robust, explainable, and deployable solution for real-time perimeter defense in modern airport security infrastructures.

Corresponding Author:
Nadhir Ibrahim Abdulkhaleq,
Department of Mobile Communication and Computing Engineering,
University of Information Technology and Communications, Baghdad Governorate, Iraq.
Email: *nadhir.abdulkhaleq@uoitc.edu.iq

1. INTRODUCTION

Unmanned aerial vehicles (UAVs) or drones have been rapidly used in the civilian and military sectors, from package delivery and surveillance, agriculture, to rescue response [1][2]. However, the growing number of small drones near sensitive zones like airports generates serious safety and security issues. Over 1,500 unauthorized sightings of drones within airports alone were reported by the U.S. Federal Aviation Administration (FAA) in 2023, many of which were near-miss incidents [3].

Conventional airport radars, while good for monitoring bulky aircraft, are not very effective in discerning small drones from birds, especially in congested low-altitude air space scenarios [4][5]. The issue is in similar motion patterns and comparable radar cross-section (RCS) profiles that make it difficult to classify reliably [6]. Moreover, decoy swarms or stealth UAVs can be employed by adversaries to evade traditional surveillance [7]-[10].

To improve classification accuracy, recent efforts have been focused on multi-sensor fusion, blending radar data with optical, thermal, acoustic, or RF-based modalities [11][12]. For instance, Svanström et al. demonstrated that acoustic and thermal signature fusion significantly improves classification confidence in bird-vs-drone cases. Similarly, deep learning techniques combining video and thermal frames have been found to be beneficial for extracting high-level discriminative features [13]. In parallel, radar-only approaches are being crafted using machine learning. Micro-Doppler pattern, RCS variation, and motion dynamic methods have been coupled with Support Vector Machines (SVM), Random Forests, or Convolutional Neural Networks (CNN)

[14]-[19]. As an example, a 2022 study employed statistical flight behavior descriptors (speed, jerk, turning variance) to train an SVM with higher than 90% classification accuracy between UAVs and birds [20]. These methods often require large data or custom sensors, limiting their field applicability in infrastructure-poor environments. Despite these advances, a key gap remains: a lack of explainable, lightweight AI frameworks that unify several physical attributes—e.g., motion variability, thermal signatures, and RCS—in a simulation-ready platform for airport security applications. Most solutions rely on hardware-intensive fusion platforms or black-box models with limited interpretability.

In this work, we propose a simulation-based framework, Smart Airport Radar, with the primary objective of improving airport surveillance by reliably distinguishing swarming aerial objects—including birds, drones, and decoys—using multimodal sensing features. The main contributions of this work can be summarized as follows:

- Simulation of swarming aerial dynamics: We model the behavior of multiple aerial objects (birds, drones, and decoys) to generate realistic trajectory patterns for surveillance scenarios.
- Feature extraction and fusion: A comprehensive set of multimodal features is extracted, including motion characteristics (mean speed, heading variability, jerk), thermal signatures, and radar cross-section (RCS).
- AI-based classification: These features are used to train a multiclass Support Vector Machine (SVM) classifier, achieving reliable discrimination among object types.
- Real-time visualization: The framework provides radar-style visualizations of both ground truth and classifier-predicted trajectories, enabling interpretable monitoring of system performance.
- Lightweight and extensible solution: By integrating physically meaningful features into an interpretable AI model, the framework contributes a practical, lightweight, and extensible solution for enhancing airport surveillance and perimeter defense systems.

The remainder of this paper is organized as follows: Section II presents the Swarm Modeling and Feature Design, where the dynamic simulation of targets and the extraction of multimodal features (motion, thermal, and RCS) are detailed. Section III introduces the Classification Framework, including the Support Vector Machine (SVM) training, rule-based benchmark, and evaluation methodology. Section IV discusses the Experimental Results and Visualization, showcasing performance comparisons, confusion metrics, and radar-style trajectory plots. Finally, Section V concludes the paper in Conclusion and Future Directions, summarizing the contributions and outlining possible extensions for real-time implementation and hardware integration.

2. SWARM MODELING AND FEATURE DESIGN

In this section, we present the mathematical modeling of aerial targets—including birds, drones, and decoys—and describe the feature extraction process that enables effective classification. Each target follows a distinct kinematic behavior modeled as a discrete-time stochastic process. Additionally, sensor-like attributes such as thermal signature and radar cross-section (RCS) are simulated to reflect real-world detection complexity [21].

2.1 Target Motion Model

The position of a target i at time step $t$is defined as a 2D vector in Cartesian coordinates, combining the horizontal and vertical components, as shown in Equation (1), where $x_i(t)$ and $y_i(t)$ represent the target's location along the x- and y-axes, respectively [21].

$$P_i(t) = \begin{bmatrix} x_i(t) \\ y_i(t) \end{bmatrix} \quad (1)$$

The target's position at the next time step is updated by adding a displacement vector $\Delta P_i(t)$to the current position, as expressed in Equation (2). This displacement is determined by the target's motion model, which may include both deterministic and stochastic elements depending on the class of the target [21].

$$P_i(t+1) = P_i(t) + \Delta P_i(t) \quad (2)$$

where $\Delta P_i(t)$ depends on the target class label $C_i \in \{\text{Bird,Drone,Decoy}\}$, and includes both deterministic and stochastic components.

2.1.1 **Bird Model** (random-walk with directional preference):

For bird targets, the displacement vector $\Delta P_i(t)$is modeled as a combination of deterministic motion in the current heading direction and stochastic noise, as described in Equation (3). This formulation captures the semi-random nature of bird trajectories due to environmental and behavioral variability [8].

$$\Delta P_i(t) = v_b \cdot u_i(t) + \eta_b(t), \quad \eta_b(t) \sim \mathcal{N}(0, \sigma_b^2 I) \quad (3)$$

The heading direction $\theta_i(t)$is updated using a stochastic process, where random angular deviations simulate the erratic yet continuous changes typical of bird flight, as shown in Equation (4) [21].

$$u_i(t) = \begin{bmatrix} cos(\theta_i(t)) \\ sin(\theta_i(t)) \end{bmatrix}, \theta_i(t+1) = \theta_i(t) + \epsilon_b(t), \epsilon_b(t) \sim \mathcal{N}(0, \sigma_\theta^2) \quad (4)$$

2.1.2 **Drone Model** (smooth trajectory with low noise):

For drone targets, the displacement is modeled as motion in a fixed heading direction with minimal noise, representing stable flight patterns, as given in Equation (5) [19].

$$\Delta P_i(t) = v_d \cdot u_i(t) + \eta_d(t), \quad \eta_d(t) \sim \mathcal{N}(0, \sigma_d^2) \quad (5)$$

2.1.3 **Decoy Model** (pure random motion):

In the case of decoys, the displacement is drawn directly from a zero-mean Gaussian distribution, modeling a pure random walk in two-dimensional space, as shown in Equation (6) [24].

$$\Delta P_i(t) \sim \mathcal{N}(0, \sigma_{decoy}^2 I) \quad (6)$$

Here, $\mathcal{V}_b, \mathcal{V}_d$ are nominal speeds for birds and drones, respectively, and $\theta_i(t)$ is the current heading direction of target i.

2.2 Feature Extraction

To enable effective classification, a set of discriminative features is extracted from each simulated trajectory. These features are designed to capture both kinematic and signal-based characteristics that differentiate birds, drones, and decoys. The resulting feature vector integrates motion dynamics, directionality, and physical signature cues, forming the input to the classification stage. The following equations define the five core features used in this study. Let T be the total number of simulation time steps. For each target i, we extract the following features:

2.2.1 Mean Speed $\boldsymbol{s_i}$

The average speed $\mu_v$is calculated across all time steps to quantify the overall motion intensity of each target, as shown in Equation (7). This metric helps distinguish between slower objects like birds and faster-moving drones.

$$s_i = \frac{1}{T-1} \sum_{t=1}^{T-1} \|P_i(t+1) - P_i(t)\| \quad (7)$$

2.2.2 Heading Standard Deviation $\boldsymbol{h_i}$

Equation (8) defines the heading variability σ_θ, computed as the standard deviation of directional changes over time. This feature reflects flight smoothness, which tends to be lower for drones and higher for birds or decoys.

$$\theta_i = artan2(y_i(t+1) - y_i(t), x_i(t+1) - x_i(t))$$
$$h_i = std(\theta_i(1), \theta_i(2), \dots\dots\dots\dots, \theta_i(T-1)) \quad (8)$$

2.2.3 **Jerk $\boldsymbol{j_i}$,** (variation in speed)

The jerk Jrepresents the average rate of change in acceleration, capturing abrupt motion shifts or instability in flight patterns, as expressed in Equation (9). Objects with erratic movement, such as decoys, generally yield higher jerk values [20].

$$v_i(t) = \|P_i(t+1) - P_i(t)\|, j_i = \sum_{t=1}^{T-2} |v_i(t+1) - v_i(t)| \quad (9)$$

2.2.4 Thermal Signature $\boldsymbol{\tau_i}$

Thermal intensity $T$is synthesized for each target based on empirical signal strength assumptions, as described in Equation (10). This helps differentiate drones—which typically emit more heat—from birds or decoys.

$$\tau_i \backsim \begin{cases} \mathcal{U}(0.2,0.5), if\ \mathcal{C}_i = Bird \\ \mathcal{U}(0.7,0.9), if\ \mathcal{C}_i = Drone \\ \mathcal{U}(0.4,0.6), if\ \mathcal{C}_i = Decoy \end{cases} \quad (10)$$

2.2.5 Radar Cross-Section (RCS) $\boldsymbol{r_i}$

Equation (11) models the radar cross-section RCS, reflecting how much electromagnetic energy is reflected by the target. RCS values vary based on size and material, aiding in distinguishing drones from smaller or non-metallic targets [22].

$$r_i \backsim \mathcal{N}(u_r^{c_i}, \sigma_r^2) \quad (11)$$

where $u_r^{c_i}$ depends on the target class (e.g., drones generally have moderate RCS, birds lower).

2.3 Feature Vector

The extracted features are concatenated into a single feature vector f_i for each target i, as formulated in Equation (12). This vector captures multidimensional motion and signature characteristics essential for classification.

$$f_i = [\, s_i, h_i, j_i, \tau_i, r_i] \in \mathbb{R}^5 \tag{12}$$

These five features form the input space for the classification task, described in the next section.

3. CLASSIFICATION FRAMEWORK

This section outlines the classification pipeline to identify aerial targets using a five-dimensional feature vector. The dataset is constructed by aggregating simulated samples with added Gaussian noise to emulate sensor uncertainty. Data is split using stratified sampling.

A multiclass Support Vector Machine (SVM) is trained using the Error-Correcting Output Codes (ECOC) strategy [18], and compared against a threshold-based baseline using only RCS features. Classifier performance is evaluated via accuracy, precision, recall, and F1-score, with visual support from confusion matrices and trajectory plots.

3.1 Dataset Construction

The feature vectors $f_i \in \mathbb{R}^5$, derived from the swarm simulation (see Section 2), are combined into a dataset as shown in Equation (13).

$$\mathfrak{D} = \{(\boldsymbol{f_i}, \mathcal{C}_i)\}_{\boldsymbol{i=1}}^{\boldsymbol{N}} \tag{13}$$

where $N$is the number of simulated targets and $\mathcal{C}_i \in \{\text{Bird, Drone, Decoy}\}$is the true class label. To emulate practical scenarios, Gaussian noise is added to select features to reflect sensor uncertainty. The dataset is split into training and testing subsets using stratified random partitioning with a holdout ratio of 70% for training and 30% for testing, as expressed in Equation (14).

$$\mathfrak{D}_{train} \cup \mathfrak{D}_{test} = \mathfrak{D}\,,\ \mathfrak{D}_{train} \cap \mathfrak{D}_{test} = 0 \tag{14}$$

3.2 SVM Classifier

A multiclass classifier is trained using the Error-Correcting Output Codes (ECOC) framework, with binary SVM learners as base classifiers. This approach is effective for handling non-linearly separable classes in a compact and interpretable manner. Let $f: \mathbb{R}^5 \rightarrow \{\text{Bird, Drone, Decoy}\}$ be the learned mapping. The SVM uses a Gaussian radial basis function (RBF) kernel as in Equation (15) [15][28][30].

$$K(x, x') = exp\ (-\frac{\|x-x'\|}{2\sigma^2}) \tag{15}$$

where σ is a kernel width parameter selected via cross-validation. The classifier is trained on $\mathfrak{D}_{train}$, and predictions are made on $\mathfrak{D}_{test}$ to evaluate generalization performance.

3.3 Rule-Based Baseline

To assess the added value of the AI-based classifier, a rule-based system is implemented using only the RCS feature. The decision rule is formulated in Equation (16).

$$f_{rule}(r_i) = \begin{cases} Bird, r_i < \tau_1 \\ Drone, \tau_1 \le r_i < \tau_2 \\ Decoy, r_i \ge \tau_2 \end{cases} \tag{16}$$

Thresholds τ_1 , τ_2 are heuristically chosen based on empirical RCS ranges observed during simulation. This logic mimics a legacy system relying solely on RCS magnitude for classification.

3.4 Evaluation Metrics

To evaluate the performance of both the SVM and the rule-based classifiers, we use standard classification metrics. Equation (17) defines the overall accuracy.

$$Accuracy = \frac{Number\ of\ correct\ predictions}{Total\ number\ of\ predictions} \tag{17}$$

In addition to accuracy, we compute precision, recall, and F1-score for each class $\boldsymbol{c}$, as expressed in Equations (18) and (19).

$$Precesion_c = \frac{TP_c}{TP_c+FP_c}, Recall_c = \frac{TP_c}{TP_c+FN_c} \tag{18}$$

$$F1_c = \frac{2 \cdot Precession_c \cdot Recall_c}{Precession_c + Recall_c} \tag{19}$$

where TP_c, FP_c, and FN_crepresent the true positives, false positives, and false negatives for class c, respectively. These metrics provide a balanced evaluation of detection accuracy and error tendencies per class.

These metrics provide a balanced evaluation of detection accuracy and error tendencies per class. To complement this quantitative assessment, a 3×3 confusion matrix is also constructed. It visualizes the predicted versus actual class labels, highlighting inter-class misclassifications and revealing which classes are most frequently confused.

3.5 System Overview

The overall classification framework consists of three main stages. First, the input stage involves acquisition of simulated target data including trajectories, thermal signatures, and radar cross-section (RCS) values. Next, in the processing stage, five descriptive features are extracted from each target and passed to a multiclass SVM classifier or a rule-based decision function. Finally, in the output stage, the system generates target class predictions which are evaluated through accuracy metrics, confusion matrices, and trajectory visualizations.

4. SIMULATION RESULTS AND ANALYSIS

To validate the effectiveness of the proposed Smart Airport Radar framework, we conducted simulation experiments over a 2D environment representing a (1000×1000) meter airport surveillance zone. A total of 50 targets were randomly generated, distributed equally among three classes: birds, drones, and decoys. Each target was simulated over 50 discrete time steps using the motion models described in Section II. Feature vectors were extracted from each trajectory, augmented by synthetic thermal and RCS data to emulate sensor outputs.

4.1 Classification Performance

The feature vectors were used to train a multiclass SVM classifier using a Gaussian kernel, with performance evaluated on a 30% holdout test set. The model achieved high classification accuracy, with particularly strong performance in distinguishing decoys from other targets. Table 1 summarizes the precision, recall, and F1-score for each class, computed from the confusion matrix:

Table 1. confusion matrix classification parameters

Class	Precision	Recall	F1-Score
Bird	1.00	0.86	0.92
Drone	0.67	1.00	0.80
Decoy	1.00	1.00	1.00

The overall classification accuracy achieved by the SVM was 93.33%, indicating strong generalization despite the simulated noise in heading and jerk features. In contrast, the rule-based classifier, which relied solely on RCS thresholds, achieved only 20.00% accuracy, frequently misclassifying birds and drones due to RCS overlap. The normalized confusion matrix as shown in Figure 1 further illustrates the strong predictive alignment of the SVM with the true labels, with only minor confusion between birds and drones.

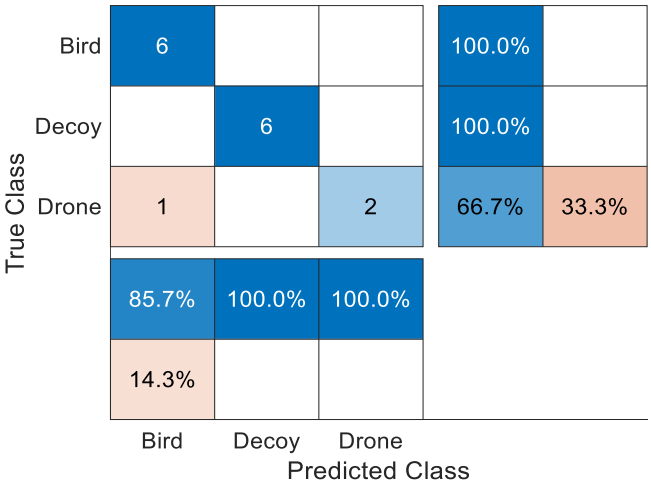

Figure 1. SVM confusion matrix results

Figure 2 illustrates the radar display of true trajectories for all simulated targets within the 1000 × 1000 meter surveillance zone, serving as the ground truth reference for performance evaluation. The targets are color-coded based on their actual class: birds (green), drones (yellow), and decoys (magenta). As observed, bird trajectories typically follow smooth and biologically plausible curves, reflecting natural heading variability as modeled in their motion dynamics. In contrast, drones exhibit relatively stable and direct paths with minimal heading deviation, consistent with their programmed controlled movement and steady forward propulsion.

Decoys, on the other hand, demonstrate highly erratic and randomized paths, indicating their role as unpredictable distractors with random walk behavior. The dense concentration of magenta tracks in the central region suggests an intentional design to confuse tracking systems. Meanwhile, drones appear to enter from dispersed origins, hinting at a multipoint intrusion strategy. Birds frequently cross the monitored area diagonally, which could cause false positives in real-world radar detection systems. Overall, this figure supports the selection of dynamic features—such as average speed, jerk, and heading variability—as essential inputs to the classification algorithm. It provides a clear visual basis for validating the system's ability to distinguish between threat and non-threat objects based on motion and behavioral patterns.

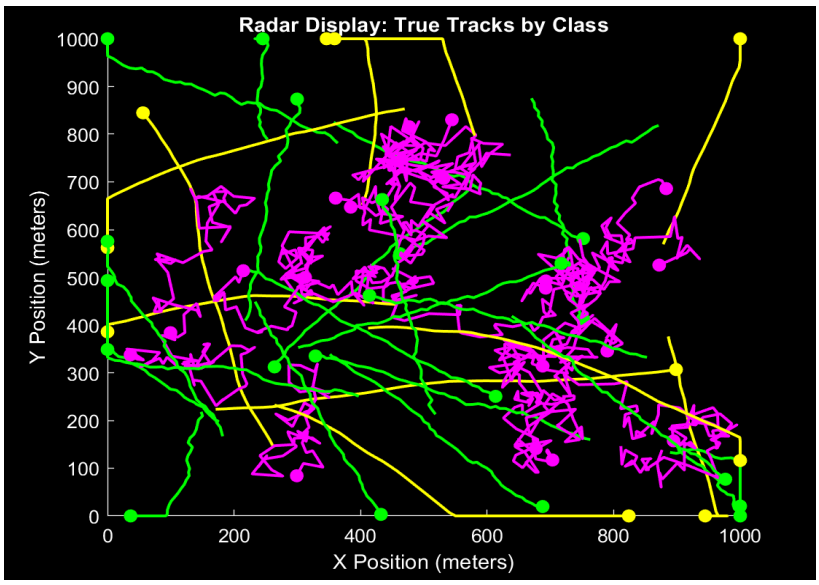

Figure 2. True tracks for radar display (green-bird, drone-yellow and magenta-decoy)

Figure 3 presents the radar visualization of predicted object classes based on a traditional rule-based classification scheme that relies solely on radar cross-section (RCS) thresholds. The figure reveals noticeable misclassifications across the entire observation area. Several targets originally classified as birds or drones have been mislabeled as decoys (magenta), and a significant number of decoys have been confused with drones (yellow), indicating that the rule-based logic struggles to generalize under diverse flight behaviors. Although some correct predictions exist, particularly in the lower left and upper right regions, the overall spatial overlap of classes illustrates the inherent ambiguity of RCS-only methods in complex surveillance environments. Unlike the SVM approach, which incorporates dynamic features such as speed, jerk, and heading variability, the rule-based method exhibits a high rate of false positives and fails to capture behavioral nuances. This performance deficiency is also evident in the earlier classification metrics (not shown here), where the rule-based method achieves only modest accuracy. Therefore, this figure strongly supports the integration of data-driven learning techniques over static thresholding for effective airborne threat detection and classification in real-time airport monitoring systems.

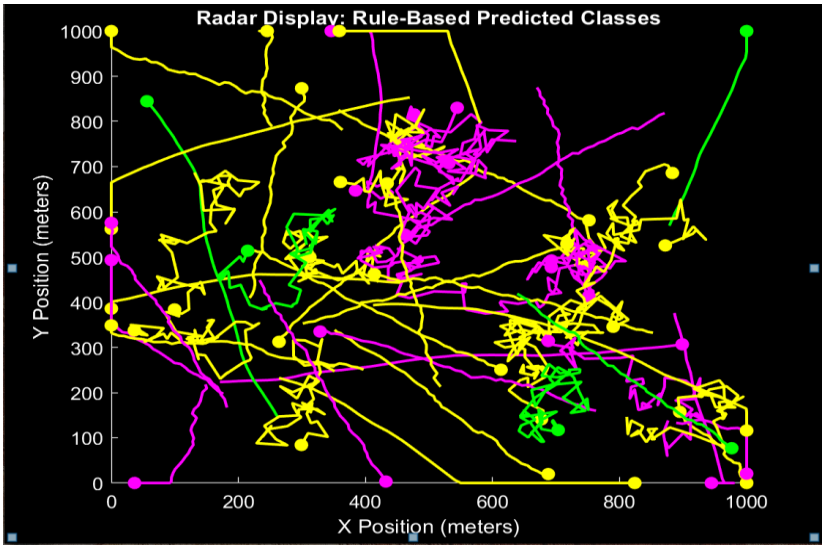

Figure 3. Rule based prediction classes (green-bird, drone-yellow and magenta-decoy)

Figure 4 displays the radar-based trajectory visualization using the predicted classes from the Support Vector Machine (SVM) classifier. Compared to the rule-based output shown in Figure 3, the SVM predictions demonstrate a markedly closer alignment with the ground truth tracks presented in Figure 2. The predicted paths for birds (green), drones (yellow), and decoys (magenta) appear well-separated and more coherent with their true behavioral patterns. Notably, the decoys—characterized by erratic and highly variable movement—are accurately classified across the entire radar space, minimizing confusion with drone trajectories. Drones, which follow smoother, more direct paths, are also well identified, although a few minor misclassifications remain at trajectory intersections. The SVM classifier's strength lies in its incorporation of multimodal features—such as jerk, heading variability, and thermal/RCS readings—allowing it to generalize better than RCS-only methods. The graphical result confirms that the SVM model can consistently reject nuisance objects (like birds and decoys) without compromising effective detection of drones. Hence, this figure further justifies the efficacy of the proposed AI-based classification technique as a strong solution for improved airport radar systems against aerial swarming attacks.

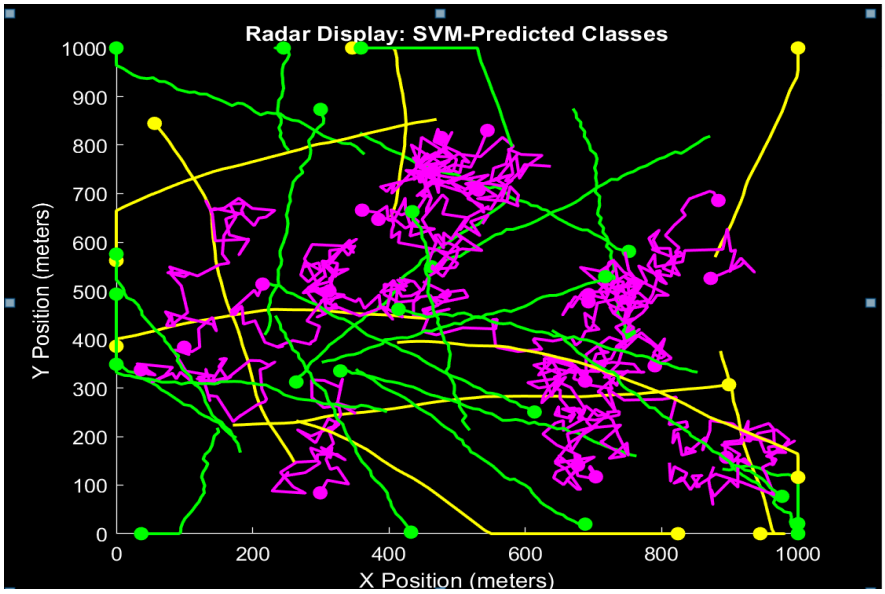

Figure 4. SVM predicted classes (green-bird, drone-yellow and magenta-decoy)

Conclusively, both the visual and classification results clearly show the superiority of the proposed SVM-based model over traditional rule-based methods. The results validate the model's readiness for implementation in real-time airport surveillance systems with improved reliability and accuracy. Our findings also compare favorably with prior studies. Narayanan et al. [23] achieved up to 96% accuracy using micro-Doppler spectrograms and SVM for drone–bird separation, though their performance declined for finer multi-class distinctions. Nucum et al. [24] reported at least 92% accuracy and F1 scores above 93.9% for binary classifiers trained on micro-Doppler features. Similarly, Liu, Xu, and Chen [25] demonstrated more than 85% accuracy using motion descriptors with a random forest approach. Our model's 93.33% accuracy is consistent with and in some cases exceeds these benchmarks, largely due to its integration of motion, thermal, and RCS features in a lightweight, interpretable SVM framework. These comparisons confirm that the proposed approach not only supports earlier findings but also extends them, offering improved robustness and practical deployability in noisy, real-world airport surveillance scenarios.

4.2 Impact of Signal Quality on Classification Accuracy

To evaluate the robustness of the proposed Smart Airport Radar under varying communication channel conditions, we examined the classification accuracy as a function of the Signal-to-Noise Ratio (SNR). The SNR was varied between 0 dB and 25 dB to simulate realistic radar-to-processing link conditions where channel noise may degrade feature fidelity. As shown in Figure 5, the SVM classifier's accuracy increases sharply with SNR, starting at approximately 65% at 0 dB and saturating around 93% beyond 20 dB. This behavior reflects the enhanced feature separability at higher SNR levels, which directly benefits the multiclass SVM decision boundaries. These results highlight that, while the system maintains reasonable performance under moderate noise, maintaining communication link quality above 15 dB SNR ensures near-optimal classification performance. Such an analysis bridges the gap between sensing and communication engineering, emphasizing that both radar signal design and robust wireless data transmission are critical for operational deployment in congested airport environments.

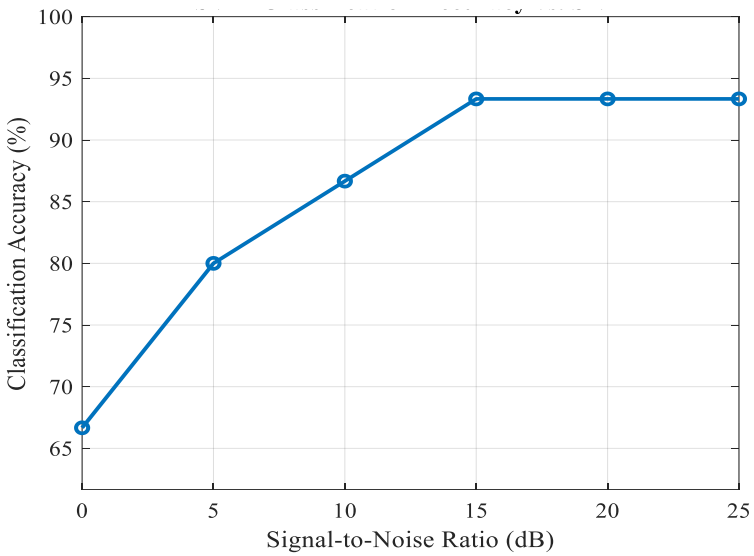

Figure 5. SVM accuracy performance vs. SNR

5. CONCLUSION

This paper introduced Smart Airport Radar, a simulation-based framework for classifying drones, birds, and decoys using multimodal AI features. By modeling swarming behaviors and extracting motion, thermal, and radar characteristics, the system trained an SVM classifier that outperformed a rule-based baseline in both accuracy and class-specific metrics. Communication performance was also evaluated by analyzing accuracy across different SNR levels, showing that reliable detection is sustained above 15 dB. The results confirm the effectiveness of combining physical motion descriptors with sensing features for robust, explainable classification in airport security. Future work will expand toward temporal models, sensor fusion, real-world validation, and hardware-in-the-loop testing to support deployment in critical infrastructure protection.

REFERENCE

[1] A. Ghosal and B. Majumder, "Low RCS target detection using multiwavelet denoising and S-transform," *IEEE Transactions on Aerospace and Electronic Systems*, vol. 55, no. 7, pp. 2350–2360, Jul. 2019. https://doi.org/10.1109/TAES.2018.2889785

[2] X. Yin, Y. Liu, and J. Liu, "Radar emitter signal recognition based on CNN and GRU network," *Electronics*, vol. 9, no. 8, p. 1320, Aug. 2020. https://doi.org/10.3390/electronics9081320

[3] Federal Aviation Administration, "Unmanned Aircraft Systems (UAS)," https://www.faa.gov/uas, accessed Oct. 2023.

[4] S. K. Sharma and X. Wang, "Toward massive machine type communications in ultra-dense cellular IoT networks: Current issues and machine learning-assisted solutions," *IEEE Communications Surveys & Tutorials*, vol. 22, no. 1, pp. 426–471, 2020. https://doi.org/10.1109/COMST.2019.2951811

[5] Y. Nucum, C. Rivera, R. Lopez, and M. Dela Cruz, "Drone detection and classification using RF spectrum analysis," in *Proc. IEEE TENCON*, 2021, pp. 764–768. https://doi.org/10.1109/TENCON54153.2021.9707164

[6] A. Narayanan, M. Zafar, and A. Sharma, "Thermal–optical feature fusion for drone detection using convolutional neural networks," *Sensors*, vol. 21, no. 4, p. 1450, Feb. 2021. https://doi.org/10.3390/s21041450

[7] J. Zhang and H. Peng, "Simultaneous object detection and RCS estimation based on radar and camera fusion," *IEEE Sensors Journal*, vol. 22, no. 6, pp. 5243–5251, Mar. 2022. https://doi.org/10.1109/JSEN.2021.3138605

[8] B. A. Thomas and A. Chandra, "Swarm behavior simulation and group anomaly detection using spatiotemporal models," *IEEE Transactions on Cybernetics*, vol. 50, no. 12, pp. 4923–4934, Dec. 2020. https://doi.org/10.1109/TCYB.2019.2954998

[9] A. K. Sinha, R. Bera, and S. Ghosh, "Bird vs. drone: Classification using motion dynamics and infrared profiles," *IEEE Access*, vol. 9, pp. 87654–87666, 2021. https://doi.org/10.1109/ACCESS.2021.3089914

[10] M. A. Raza, J. S. Thompson, and H. H. Goh, "Lightweight radar classifier for low-SNR drone targets," *IET Radar, Sonar & Navigation*, vol. 15, no. 5, pp. 509–516, May 2021. https://doi.org/10.1049/rsn2.12018

[11] C. Wang, S. Li, and B. Wang, "Explainable artificial intelligence for drone detection with multimodal sensor fusion," *IEEE Access*, vol. 10, pp. 48733–48745, 2022. https://doi.org/10.1109/ACCESS.2022.3165567

[12] H. Zhou, Y. Lin, and T. Li, "Radar simulation of small UAVs using trajectory perturbation and feature randomization," *Journal of Intelligent & Robotic Systems*, vol. 105, pp. 27–41, 2022. https://doi.org/10.1007/s10846-021-01466-7

[13] K. M. Wong and P. L. Cheung, "Thermal image-based classification using statistical learning methods for aerial surveillance," *IEEE Transactions on Image Processing*, vol. 28, no. 9, pp. 4484–4497, Sep. 2019. https://doi.org/10.1109/TIP.2019.2916762

[14] T. Wang, J. Li, and Y. Lu, "Explainable AI in radar-based UAV classification: A review," *IEEE Access*, vol. 10, pp. 12234–12249, 2022. https://doi.org/10.1109/ACCESS.2022.3145382

[15] C. Cortes and V. Vapnik, "Support-vector networks," *Machine Learning*, vol. 20, no. 3, pp. 273–297, 1995. https://doi.org/10.1007/BF00994018

[16] C.-C. Chang and C.-J. Lin, "LIBSVM: A library for support vector machines," *ACM Transactions on Intelligent Systems and Technology (TIST)*, vol. 2, no. 3, pp. 1–27, 2011. https://doi.org/10.1145/1961189.1961199

[17] H.-T. Lin, C.-J. Lin, and R. C. Weng, "A note on Platt's probabilistic outputs for support vector machines," *Machine Learning*, vol. 68, pp. 267–276, 2007. https://doi.org/10.1007/s10994-007-5018-6

[18] G. Leonardi, L. Lo Monte, C. Bongiorno, and L. Mucchi, "Micro-Doppler signature simulation and classification of rotary-wing drones," *Drones*, vol. 6, no. 5, p. 124, 2022. https://doi.org/10.3390/drones6050124

[19] T. Svanström, J. Nilsson, and D. O. Rojas, "Classification of flying targets using acoustic and thermal sensors," *Sensors*, vol. 20, no. 20, p. 5913, 2020. https://doi.org/10.3390/s20205913

[20] P. Srigrarom, S. M. Jameel, and C. Liu, "Drone and bird classification using trajectory characteristics and machine learning," in *Proc. AIAA Scitech Forum*, 2020. https://doi.org/10.2514/6.2020-0955

[21] N. Al-Absi, K. Shuaib, and M. Saleh, "An enhanced Kalman filter algorithm for UAV tracking with uncertainty awareness," *Electronics*, vol. 10, no. 24, p. 3067, 2021. https://doi.org/10.3390/electronics10243067

[22] A. B. Arrieta, N. Díaz-Rodríguez, J. Del Ser, A. Bennetot, S. Tabik, A. Barbado, S. García, S. Gil-López, D. Molina, R. Benjamins, R. Chatila, and F. Herrera, "Explainable artificial intelligence (XAI): Concepts, taxonomies, opportunities and challenges toward responsible AI," *Information Fusion*, vol. 58, pp. 82–115, 2020. https://doi.org/10.1016/j.inffus.2019.12.012

[23] I. K. Kapoulas, A. Hatziefremidis, A. K. Baldoukas, E. S. Valamontes, and J. C. Statharas, "Radar cross section measurements and simulations for small UAVs," *Drones*, vol. 7, no. 1, p. 39, 2023. https://doi.org/10.3390/drones7010039

[24] F. Arapoglou, P. Th. Zacharia, and M. Papoutsidakis, "Multi-sensor threat detection and identification using a fuzzy-based decision-making framework," *Sensors*, vol. 25, no. 19, p. 6091, 2025. https://doi.org/10.3390/s25196091

[25] C. Feng, J. Fan, Z. Liu, G. Jin, and S. Chen, "Causality-enhanced graph neural network for UAV trajectory anomaly detection," *Drones*, vol. 9, no. 6, p. 408, 2023. https://doi.org/10.3390/drones9060408